

## Article

# One-Step Synthesis of Nitrogen-Doped Porous Carbon Derived from Biomass for Lithium-Ion Battery

Bingbing Mi<sup>1</sup>, Jing Yuan<sup>1</sup>, Hecheng Li<sup>1</sup>, Wanhe Hu<sup>2</sup>, Changle Jiang<sup>2</sup>, Xianmiao Liu<sup>3</sup>, Yafang Lei<sup>1,\*</sup> and Zhijia Liu<sup>3,\*</sup>

<sup>1</sup> College of Forestry, Northwest A & F University, Xianyang 712100, China; bingbingmi@nwfu.edu.cn (B.M.)

<sup>2</sup> School of Natural Resources, West Virginia University, Morgantown, WV 26506, USA

<sup>3</sup> International Centre for Bamboo and Rattan, Beijing 100102, China

\* Correspondence: leiyafang@sina.com (Y.L.); liuzj@icbr.ac.cn (Z.L.)

**Abstract:** Bamboo shoot is renewable biomass rich in carbon and nitrogen. To take advantage of its sources of carbon and nitrogen, hierarchical porous nitrogen-doped carbon materials derived from bamboo shoot were acquired via a one-step method in this study. The obtained carbons were characterized by using XRD, Raman, N<sub>2</sub> sorption, SEM, TEM, XPS, etc. The carbon calcinated at 700 °C with KHCO<sub>3</sub> treatment (BSC) displays a large surface area (1475.5 m<sup>2</sup> g<sup>-1</sup>) and typically porous structure from micro- to macropores, a self-nitrogen content, and many defects, which could offer transport channels and active sites for lithium ions while used as carbon anode. Based on the above features and the synergistic effects among them, BSC exhibits the typical electrochemical performance of a carbon-based anode material, with a specific capacity as high as 611.3 mA h g<sup>-1</sup> (a Coulombic efficiency of 98.7%) after 100 cycles at a current density of 0.1 A g<sup>-1</sup>. Meanwhile, it also has a good rate performance and excellent cycling properties (436.1 mA h g<sup>-1</sup> after 300 cycles at 0.1 A g<sup>-1</sup>) compared with NBSC (carbon directly carbonized at 700 °C). Thus, it is promising for further improvements made to porous carbon derived from biomass and used as anode in the application of energy storage, and could be a guideline for the preparation of high-value-added carbon materials derived from biomass.

**Keywords:** porous carbon; biomass; lithium-ion battery; anode; electrochemical properties



**Citation:** Mi, B.; Yuan, J.; Li, H.; Hu, W.; Jiang, C.; Liu, X.; Lei, Y.; Liu, Z. One-Step Synthesis of Nitrogen-Doped Porous Carbon Derived from Biomass for Lithium-Ion Battery. *Coatings* **2023**, *13*, 1960. <https://doi.org/10.3390/coatings13111960>

Academic Editor: Je Moon Yun

Received: 14 October 2023

Revised: 13 November 2023

Accepted: 14 November 2023

Published: 17 November 2023



**Copyright:** © 2023 by the authors. Licensee MDPI, Basel, Switzerland. This article is an open access article distributed under the terms and conditions of the Creative Commons Attribution (CC BY) license (<https://creativecommons.org/licenses/by/4.0/>).

## 1. Introduction

Lithium-ion batteries (LIBs), which have the advantages of high energy density, long cycle life, and flexibility in design, are regarded as some of the most promising devices in energy storage. LIBs have a wide application in portable electronic devices, such as computers, mobile phones, and electric vehicles [1–4]. However, the limited energy density of LIBs makes them difficult to apply to some high-demand pieces of equipment. As a component of LIBs, anode materials, especially those composed of carbonaceous materials, have been studied by scholars for a long time. Graphite, as it is well known, is the most commonly used anode material. However, its low theoretical capacity of 372 mA h g<sup>-1</sup> cannot meet the demands of markets [5]. In recent years, porous carbon materials doped with nitrogen (N) atoms have shown superior electrochemical performance because N atoms can supply enough Li-ion storage sites and enhance reactivity [6–10]. The radius of a N atom is closer to that of a C atom, which means it is much more easily inserted into the lattice of carbon than of other atoms. Additionally, doping with N atoms could change the atom connection and tunnel structure to enhance hydrophilicity, resulting in increasing the electronic transmission rate and the active sites on the surface of the carbon materials. Selvamani et al. [11] illustrated nitrogen-doped fish scale hierarchical carbon as an anode material, which had a steady reversible capacity of 483 mA h g<sup>-1</sup> at 75 mA g<sup>-1</sup> in organic electrolytes. They also found that N atoms, especially pyrrolic N present in graphene,

can offer enough active sites for Li-ion storage. Hou et al. [12] prepared nitrogen-doped carbon nanosheets derived from silk and applied them as anodes in LIBs, and the results showed a reversible lithium storage capacity of  $1865 \text{ mA h g}^{-1}$ . Several approaches could be used to prepare nitrogen-doped carbon materials, such as hydrothermal carbonization, pyrolysis, and joint hydrothermal carbonization and pyrolysis. In this process, nitrogen-rich precursors are beneficial for the preparation of nitrogen-doped carbons, such as the commonly used  $\text{NH}_3$ , urea, melamine, and some other small-molecule substances [13–15]. However, these methods also present some shortcomings, such as high cost, multiple steps, and low nitrogen doping content, which limit their special applications. Thus, porous nitrogen-doped carbon materials with a large specific surface area could be prepared by using renewable raw materials from biomass as nitrogen and carbon precursors to achieve excellent electrochemical performance.

Biomass is an environmentally friendly and natural resource which has attracted much attention as a precursor to prepare porous carbon materials [12,16,17]. The diversity of the components and their low cost, abundant resources, rapid regeneration, and environmental friendliness provide advantages in fabricating heteroatom-doped carbon materials. Recently, types of nitrogen-rich biomass, such as honey [18], cow horns [19], fish scales [11], garlic peel [20], prawn shells [21], and butterfly wings [22], were used as precursors to fabricate nitrogen-doped carbons and have attracted much attention as anode materials for LIBs. Currently, there are two main routes for preparing porous nitrogen-doped carbon materials: one is the post-processing of porous carbons by adding additional nitrogen sources; the other is in situ doping carbon of nitrogen-rich precursors. Both routes require many steps [23,24] or require the help of soft or hard templates [18,25] or the post-activation process (e.g., activation by  $\text{H}_2\text{O}$ ,  $\text{CO}_2$ ,  $\text{KOH}$ ,  $\text{NaOH}$ , etc.) [26–28]. To some extent, these processes are costly and complicated. Also, carbon materials derived from biomass show low Li-storage behavior at relatively high current densities. Thus, it is necessary to find a route to prepare nitrogen-doped carbon materials with a large specific surface area and different pore sizes through fewer steps for superior electrochemical LIBs made from biomass.

Bamboo shoot is the bud of bamboo; it is famous for its taste and nutrition, is rich in proteins, carbohydrates, and minerals, and has a low fat content [29,30]. Most applications of bamboo shoot focus on its use as a vegetable. However, there is a lack of studies on its use as an active electrode material for LIBs based on its high N content, 4.27% [31], which might be a potential precursor for the preparation of nitrogen-doped porous carbon materials without adding an extra nitrogen source.

In this work, bamboo shoots, which could offer a source of carbon and nitrogen, were used as a precursor to prepare hierarchical porous nitrogen-doped carbon materials. A high specific surface area and porous structure were obtained by adding potassium bicarbonate ( $\text{KHCO}_3$ ) through a one-pot synthesis route, which does not require multiple steps and the assistance of a template, or through adding extra N sources. The obtained carbon materials derived from bamboo shoot exhibited excellent energy storage performance when used as the anode material for LIBs.

## 2. Materials and Methods

### 2.1. Materials

Bamboo shoots were used as a carbon and nitrogen precursor; they were obtained from Lishui, Zhejiang Province, China. The collected bamboo shoots were ground into powder after cleaning, cutting, drying, and sieving into  $250\text{--}425 \mu\text{m}$  particles.  $\text{KHCO}_3$  was used as an activator; it was purchased from Sinopharm Chemicals Co., Ltd. (Shanghai, China). The reagents and chemicals in the work were used as received without further purification.

### 2.2. Preparation of the Bamboo Shoot Derived Carbon (BSC)

The preparation process of porous nitrogen-doped carbon was similar to our previous research [31]. Briefly, 2 g bamboo shoot powder was impregnated in  $\text{KHCO}_3$  solution (the weight ratio of  $\text{KHCO}_3$  to bamboo shoot was 4) for 0.5 h under ultrasonic treatment. The

mixture was soaked for 12 h, then freeze-dried until no further change in mass. It was then calcined in a tubular furnace and held at 700 °C for 1 h under an inert gas (N<sub>2</sub>) atmosphere (heating rate: 10 °C min<sup>-1</sup>). The obtained carbon material was washed with deionized water to neutralize and dried at 75 °C. The obtained carbon derived from the bamboo shoot is named BSC. For comparison, the sample without adding KHCO<sub>3</sub> was directly carbonized at 700 °C for 1 h under the same gas atmosphere, and named NBSC.

### 2.3. Material Characterization

Different techniques were used to characterize the as-prepared carbon materials. A field emission scanning electron microscope (SEM, Hitachi S-4800, Tokyo, Japan) and transmission electron microscopy (TEM, FEI Tecnai G2 20, Stanford, CA, USA) were used to observe the morphologies of the carbon materials. An X-ray photoelectron spectrum (XPS, Thermo Scientific Escalab 250Xi, Waltham, MA, USA) was used to carry out the Vacuum Generators XPS system, operated using Al (K $\alpha$ ) radiation. In order to obtain the degree of crystallinity and graphitization of the carbons, powder X-ray diffraction patterns (XRD, Bruker D8 Advance, Mannheim, Germany) were recorded using Cu K $\alpha$  ( $\lambda = 0.15496$  nm) radiation in the  $2\theta$  range from 10° to 60°. Raman spectra were acquired on a Raman Microscope (Thermo Scientific, Waltham, MA, USA). N<sub>2</sub> sorption isotherm measurement was performed on the ASAP 2020 analyzer (Micromeritics, Norcross, GA, USA) at 77 K.

### 2.4. Electrochemical Measurements

The electrochemical performances of the bamboo-shoot-derived carbon anode material for LIBs were shown using 2025-type coin cells at room temperature. The working electrode consisted of active materials, carbon black (as the conductivity agent) and polyvinylidene fluoride (PVDF, as the binder) in a weight ratio of 80:10:10, and the solvent was N-methyl-2-pyrrolidinone (NMP). The mixture was spread on Ni mesh (diameter 10 mm), followed by drying in a vacuum oven at a temperature of 80 °C for 4 h. The counter electrode was pure lithium foil and 1 M LiPF<sub>6</sub> in ethylene carbonate (EC)-dimethyl carbonate (DMC) (1:1 by volume) as the electrolyte when lithium-ion batteries were fabricated. The lithium-ion cells were assembled in the argon-filled glovebox (with H<sub>2</sub>O < 1 ppm and O<sub>2</sub> < 1 ppm). The galvanostatic discharge–charge tests were carried out on a Land CT2001A system (Wuhan, China) in the voltage range of 0.01~3.0 V. Cycle voltammetry (CV) measurements were conducted on a Zennium electrochemical workstation (Zahner, Kronach, Germany) in the voltage range of 0.01 to 3.0 V, and the scanning rate was 0.1 mV s<sup>-1</sup>.

## 3. Results and Discussion

X-ray diffraction (XRD) spectra of BSC and NBSC are exhibited in Figure 1a. As shown in the picture, there are two typical peaks of the two materials located at  $2\theta = \sim 24^\circ$  and  $\sim 43^\circ$ , which are named as (002) and (100) of the pseudo-graphitic domains, respectively [32]. It can be seen that BSC has two broad diffraction peaks, indicating that it is a typical carbon with a low graphitization degree [19]. This also demonstrates that BSC has a graphitic structure [16]. The structures of the two carbon materials were further investigated via Raman spectroscopy. As displayed in Figure 1b, the two samples show two peaks at around 1340 cm<sup>-1</sup> and 1580 cm<sup>-1</sup>, corresponding to the disorder-induced D-bands and in-plane vibration G-bands, respectively. As we all know, the value of  $I_D/I_G$  means the degree of graphitic ordering, including defects, edges, disorder, and carbon grain size [17,33]. The values of  $I_D/I_G$  were 1.12 for NBSC and 1.25 for BSC, respectively. The results reveal that BSC has a higher degree of disorder, more defects, and more edges than NBSC after activation, which coincides with the above analysis of XRD. This also suggests that while BSC acted as a battery anode, not only could it improve the ion-storage ability, it could also increase the reversible capacity.

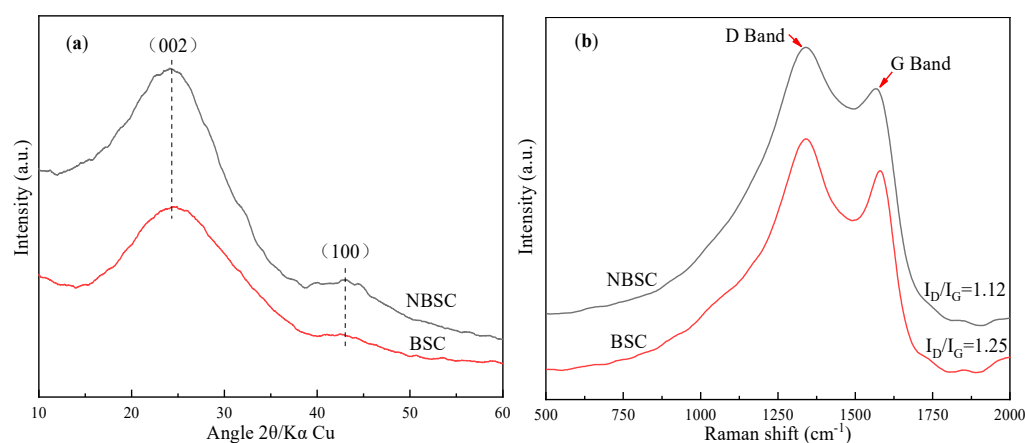


**Figure 1.** (a) XRD patterns and (b) Raman spectra of NBSC and BSC.

To further investigate the porous structure of BSC,  $N_2$  adsorption–desorption isotherms were assessed (Figure 2a). As depicted in Figure 2a, BSC displayed a type I adsorption isotherm, suggesting that it was a typical microporous material. There was a rapid increase within the relative pressure of 0~0.3, due to the micropores filling. Subsequently, a stable trend appeared at the relative pressure of 0.3~0.9, indicating there was no or little further adsorption, and that there might also be narrower mesopores; this result coincided with an average pore size of 1.97 nm. Additionally, there were tails around a relative pressure of 1.0, implying the existence of macropores. Thus, the obtained carbon of BSC had hierarchically porous structures from the micro to macro level. According to the findings of nitrogen adsorption, the carbon of BSC displays a high specific surface area ( $1475.5 \text{ m}^2 \text{ g}^{-1}$ , calculated by BET method), the total pore volume is found to be  $0.73 \text{ m}^3 \text{ g}^{-1}$ , the micropore volume  $0.63 \text{ m}^3 \text{ g}^{-1}$ , and the meso-/macropore volume  $0.10 \text{ m}^3 \text{ g}^{-1}$ . Compared with the specific surface area of biomass-based carbon materials, such as ox horn [19], shrimp shells [23], and wheat straw [34], BSC possessed a larger specific surface area. However, the specific surface area of NBSC was very little ( $4.6 \text{ m}^2 \text{ g}^{-1}$ ) [31], indicating only a few pores in it. In addition, the percent of the micropores of BSC reached 86.4%. It is well known that micropores play an important role in rapid electrolyte transfer as battery anodes, offering a favorable pathway for the penetration and transport of ions [35]. The pore size distribution curves (PSDs) of BSC were calculated via NLDFT and are shown in Figure 2b. It was evident that the pore size distribution of BSC is mainly concentrated at around 0.5~2 nm. Some pore sizes over 2 nm also can be observed. Previous research reported that materials with a high specific surface area and hierarchical pore structures could show superior electrochemical performance [10,36]. Thus, the obtained carbon of BSC is expected to have better behavior while acting as the anode material for Li-ion batteries.

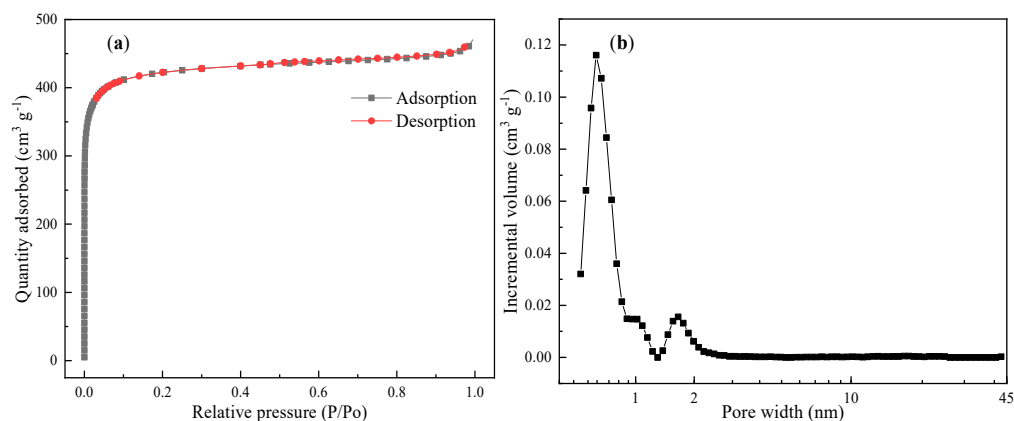


**Figure 2.** (a) Nitrogen sorption isotherms and (b) pore size distribution curves of BSC.

SEM images of freeze-dried bamboo shoot, the carbon obtained at 700 °C (NBSC), and the carbon derived from KHCO<sub>3</sub>-treated bamboo shoots (BSC) are depicted in Figure 3. Figure 3a displays that bamboo shoot is composed of hollow cells with thin walls, the cell wall is thinner and the cell cavity is independent of adjacent cells. Moreover, abundant starch grains can be seen in the cell cavity. The results can also be demonstrated by the larger magnification image of Figure 3b. To some extent, the hollow structure and substance are helpful in preparing carbon materials with a high specific surface area [37]. Figure 3c,d show the images of the obtained carbon calcinated at 700 °C without KHCO<sub>3</sub> treatment (NBSC). As can be seen, the cell wall collapsed and thickened, and starch grains disappeared after carbonization. However, some of the original structure of the cell also remained. Figure 3e,f are the images of BSC. Numerous pores existed on the surface of BSC; these pores intersected with each other to form different channels, which could provide more space for electrolyte diffusion (Figure 3c). From the high magnification of Figure 3f, it is also shown that there are pores of different sizes on the surface of BSC. Some of the pores, especially the small ones, collapsed to form large pores, suggesting that the addition of KHCO<sub>3</sub> and pyrolysis at high temperature could increase the specific surface area and change the pore sizes. These results are also consistent with the aforementioned N<sub>2</sub> adsorption results in this work. NBSC and BSC were further characterized via TEM, as displayed in Figure 4a,b. As shown in the TEM images, few pores could be seen in NBSC (Figure 4a), but different size pores and collapsed pore structures could be seen in BSC (Figure 4b). Compared to granular structures, these different size pores are favorable for electronic transport. The TEM images further reveal the details of the amorphous structures of BSC, which is consistent with the results of SEM.

XPS was used to analyze the compositions and the forms of different bonds of the obtained carbon materials. From Figure 5a, three peaks can be seen situated at 283.8 eV, 398.5 eV, and 531.1 eV, corresponding to the spectra of C1s, N1s, and O1s, respectively. The atomic percentages of C1s, N1s and O1s are 87.67%, 4.92% and 7.41%, respectively. As depicted in Figure 5b, the C1s spectrum was divided into three peaks, located at 284.9 eV, 286.4 eV, and 288.9 eV. The peak at 284.9 eV corresponds to sp<sup>2</sup> hybridized C-C, the peak at 286.4 eV is due to the C-N group, and the peak at 288.9 eV is attributed to O=C-O bonding. The results further confirmed the presence of N and O functional groups on the surface of BSC [23]. It is well known that nitrogen has a smaller atomic diameter than carbon, which means it has a higher electronegativity and is more favorable for Li-ion storage. Besides, due to the presence of nitrogen, more defects were generated and more active sites were offered for ion storage [38]. The N1s spectrum of BSC in Figure 5c can be divided into four peaks, consisting of N-oxide (N-X at 404.8 eV), quaternary N (N-Q at 401.3 eV), pyrrolic N (N-5 at 400.3 eV) and pyridinic N (N-6 at 398.5 eV), respectively. Pyridinic N is more beneficial than pyrrolic N for Li-ion storage and reversible capacity [19,39,40]. The content of pyridinic N (14.1%) is a little lower than that of pyrrolic N (37.6%), which would have an influence on the mutual conversion between electrical energy and chemical energy. After the treatment with KHCO<sub>3</sub> at a temperature of 700 °C, the nitrogen content decreased from 4.40% to 2.79%, suggesting that the nitrogen-containing gases or organic molecules probably formed via the degradation of the nitrogen-containing groups [31], and this coincides with previous reports [41,42]. The nitrogen content could remain at 2.79% at the temperature of 700 °C; this not only could reduce the formation of the SEI film by restraining the electrolyte decomposition, but could also decrease the surface side reactions of the electrodes with the electrolyte [19]. Figure 5d shows that the O1s spectrum possesses three peaks located at 531.2 eV, 532.4 eV, and 533.3eV, mainly the varieties of oxygen functional groups, corresponding to C=O, O-C-O, and O=C-O, respectively. Compared with N on the surface of BSC, O could also increase the intensity of disorders and defects, which is beneficial for Li-ion storage [43]. It can be found from the above analysis that the as-obtained nitrogen-doped carbon of BSC possessed an abundance of disorders, morphologies, pore structures, and chemical compositions, and is expected to be a high-quality anode material for LIBs.

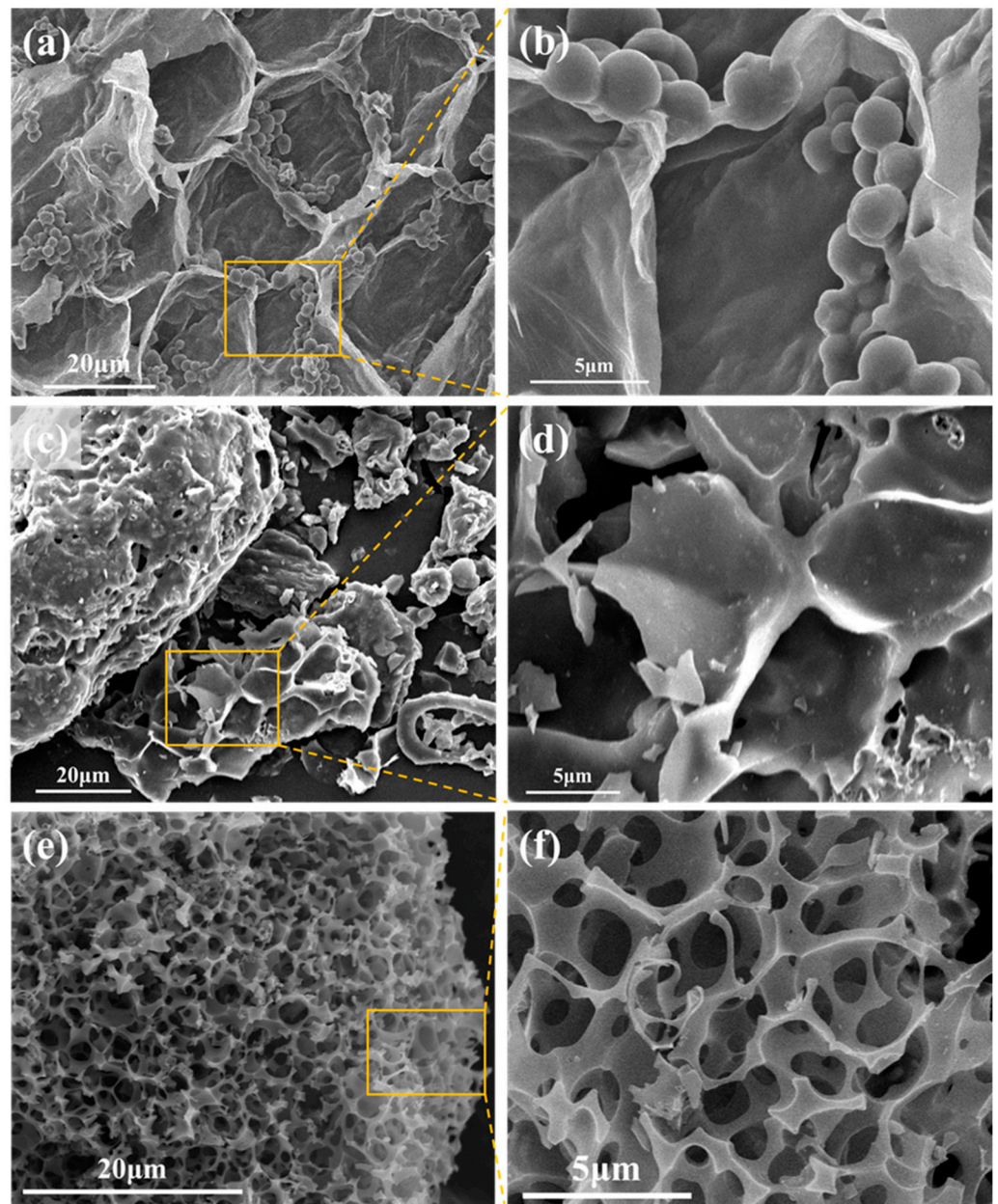


Figure 3. SEM images of (a,b) Freeze-dried bamboo shoot, (c,d) NBSC, and (e,f) BSC.

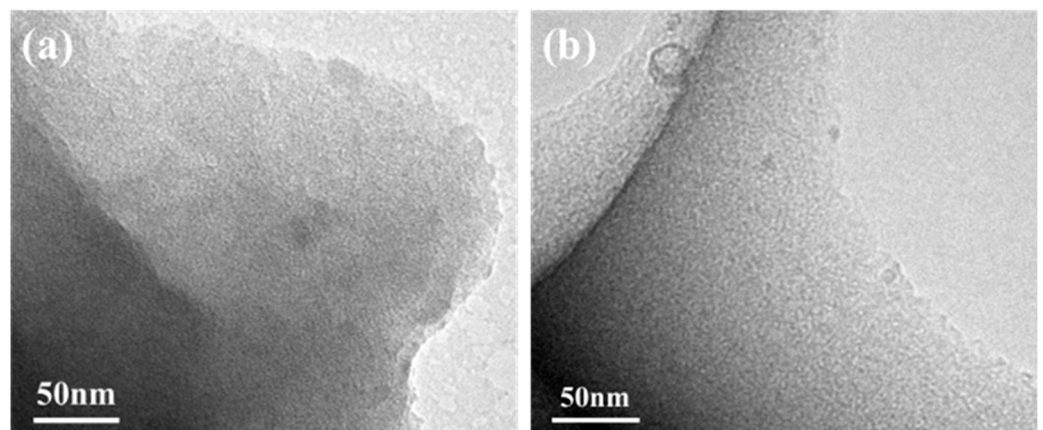
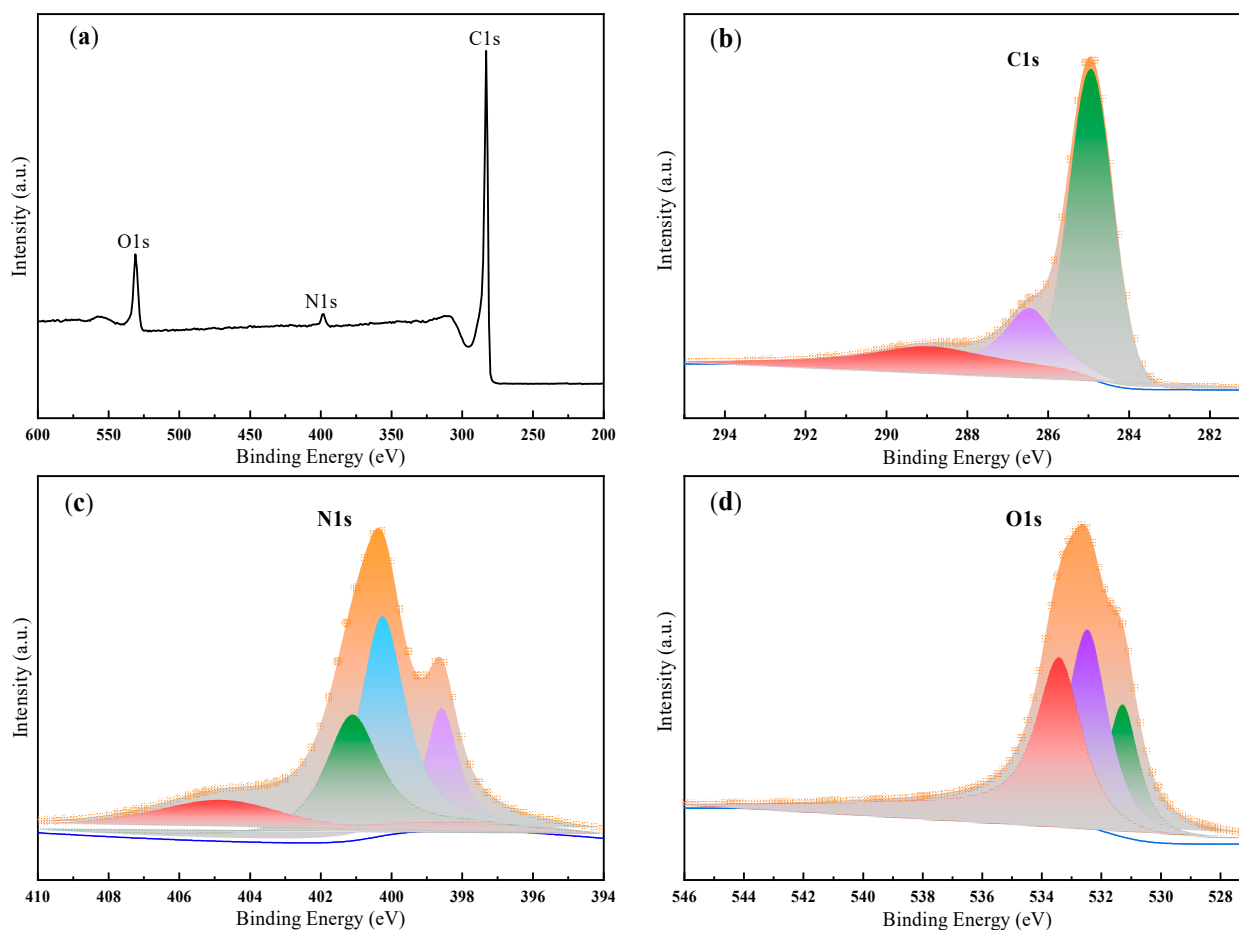


Figure 4. TEM images of (a) NBSC and (b) BSC.



**Figure 5.** (a) XPS survey spectrum, (b) C1s spectrum, (c) N1s spectrum, and (d) O1s spectrum of BSC.

To evaluate the electrochemical performance of BSC, 2025-type coin cells were assembled in the argon-filled glovebox. Figure 6 shows the cyclic voltammetry (CV) curves of BSC for the initial three cycles at a scan rate of  $0.1 \text{ mV s}^{-1}$  in the voltage range of  $0.01\sim 3.0 \text{ V}$ . The obtained carbon-based anode material presented typical CV curves. The CV curve of the first cycle differs from the second and third cycle, especially for negative scanning. There is a pronounced cathodic peak at about  $0.02\sim 2.2 \text{ V}$  during the first cycle, which is ascribed to the ability of lithium to reversibly move in the carbon skeleton and nanoscale pore structures [14]. However, this phenomenon was not found during the following two cycles, and the intensity of the peak in the first cycle was much stronger than in the subsequent two cycles. These differences might be due to the presence of the SEI layer, the insertion of Li-ion into the active sites of BSC, and the decomposition of the electrolyte [14]. It was seen that the CV curves of the second and third cycle almost overlapped, implying the stability and good reversibility of BSC as the anode in LIB.

The first, second, third, fifth and tenth charge–discharge curves at  $0.1 \text{ A g}^{-1}$  are shown in Figure 7a,b. From Figure 7a, it can be seen that the initial discharge and charge capacities of NBSC are  $556.4$  and  $234.8 \text{ mA h g}^{-1}$ , and the initial Coulombic efficiency is  $42.2\%$ . Compared with NBSC, BSC shows higher discharge and charge capabilities. As shown in Figure 7b, the initial discharge and charge capabilities are  $1269.4$  and  $690.6 \text{ mA h g}^{-1}$ , and the initial Coulombic efficiency is  $54.4\%$ . It can be found that the BSC has high reversible capacities, which could be attributed to the hierarchically porous structure and the large specific surface area. These can provide enough electrode–electrolyte interfaces and offer more beneficial paths for the penetration and transfer of ions [38,44]. The reason for the low initial Coulombic efficiency could be the formation of a solid electrolyte interface (SEI) layer, which has an effect on the irreversible consumption of charge [40], this is the common

limit condition for most anode materials [45]. In addition, the disordered structures of BSC also have a greater effect on the larger irreversible capabilities than those of NBSC. Though a high irreversible capacity loss is presented in the first cycle, there is a tiny change in both discharge and charge curves in the following cycles, and the Coulombic efficiency of the second cycle increases sharply to 88.2% and 92.7%. In the following discharge and charge curves of NBSC and BSC, it can be clearly seen that they almost overlap, and BSC always retains a higher reversible capacity (565 mA h g<sup>-1</sup> at the 5th cycle, 549.4 mA h g<sup>-1</sup> at the 10th cycle), which further demonstrates that BSC is stable during the process of charge–discharge.

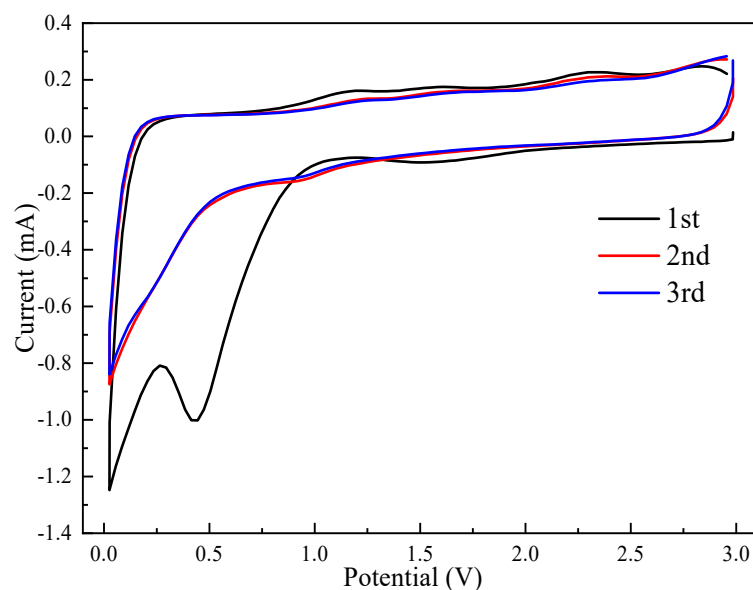


**Figure 6.** Cyclic voltammograms of BSC at a scan rate of 0.1 mV s<sup>-1</sup> for the initial three cycles.

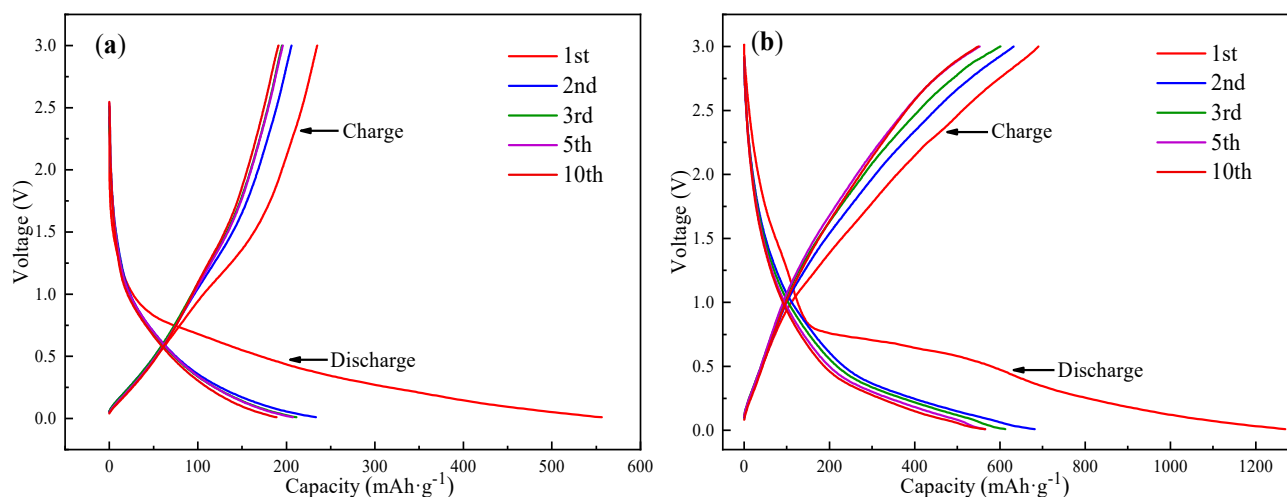


**Figure 7.** The first, second, third, fifth, and tenth charge–discharge curves of (a) NBSC and (b) BSC at a current density of 0.1 A g<sup>-1</sup>.

As one of the essential factors in evaluating electrochemical behavior, the rate capability of the obtained carbon as anodes was tested. Figure 8a shows the specific capacities of NBSC and BSC at various current densities from 0.05 to 2 A g<sup>-1</sup>. At each rate, 10 cycles of charging and discharging were performed, before 0.05 A g<sup>-1</sup> for 40 cycles. Compared with NBSC, BSC exhibits superior reversible capacities and rate capacities. Notably, at the high current density of 2 A g<sup>-1</sup>, the reversible capacity of the BSC was 180.0 mA h g<sup>-1</sup>, higher than that of NBSC (51.7 mA h g<sup>-1</sup>). When the charge–discharge was back

to  $0.05 \text{ A g}^{-1}$ , the reversible capacity of BSC at the 100th cycle maintained  $611.3 \text{ mA h g}^{-1}$ , implying that the electrodes and SEI had strong stability during the electrochemical cycling. Table 1 lists the reversible capacities of BSC at different current densities, and the corresponding capacity loss ratios with the increase in current densities from  $0.05 \text{ A g}^{-1}$  to  $2 \text{ A g}^{-1}$ . According to Figure 8a and Table 1, BSC displays better behavior than NBSC, and the reversible capacities were 868.4, 613.7, 466.6, 310.3, 240.7, and  $180.0 \text{ mA h g}^{-1}$  at current rates of 0.05, 0.1, 0.2, 0.5, 1.0 and  $2.0 \text{ A g}^{-1}$ , respectively. Additionally, when back to  $0.05 \text{ A g}^{-1}$ , BSC had a higher capacity than the other sample. It also can be found that the corresponding capacity loss ratio of BSC was lower than that of NBSC, which means the mesoporous and microporous carbons obtained at a high calcination temperature of  $700 \text{ }^\circ\text{C}$  displayed a relatively better rate capability. This can mainly be attributed to the enhancement of the degree of graphitization at a higher temperature, and defects that have a nitrogen-doping beneficial effect on the corresponding improvement in conductivity [18].

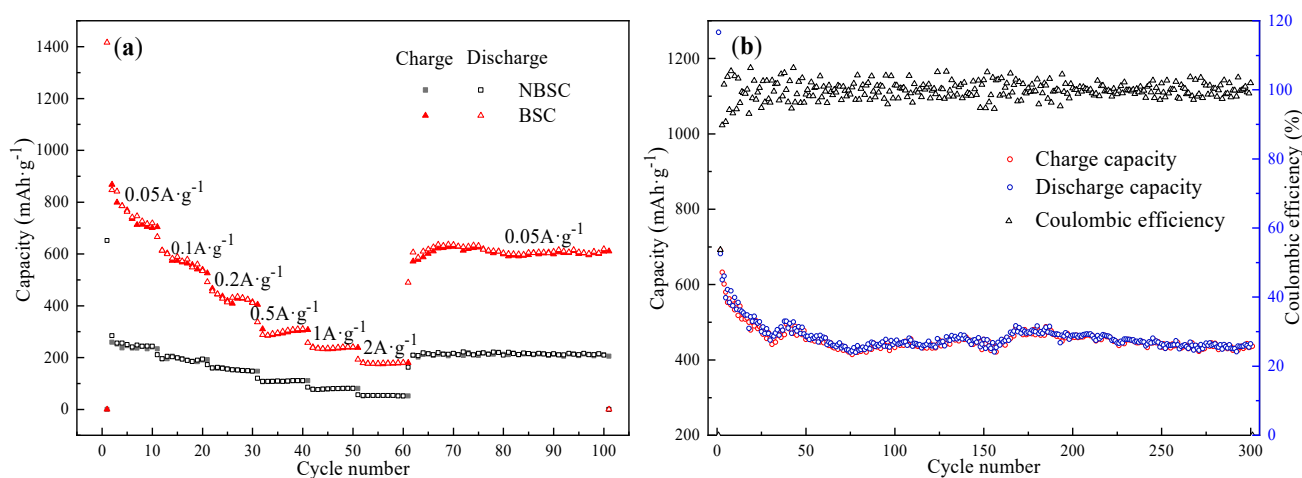


**Figure 8.** (a) Charge–discharge capacity versus cycle number of NBSC and BSC at different rates; (b) Cycling performance and corresponding Coulombic efficiency of BSC at a current density of  $0.1 \text{ A g}^{-1}$ .

**Table 1.** The reversible capacities and the corresponding capacity loss ratios of BSC at different current densities.

Current Density ( $\text{A g}^{-1}$ )	Charge Capacity ( $\text{mA h g}^{-1}$ )	Discharge Capacity ( $\text{mA h g}^{-1}$ )	Coulombic Efficiency (%)
0.05	868.4	1416.0	61.3
0.1	613.7	666.0	92.1
0.2	466.6	491.7	94.9
0.5	310.3	337.2	92.0
1.0	240.7	257.7	93.4
2.0	180.0	192.8	93.4
0.05	611.3	619.1	98.7

The cycling performance and corresponding Coulombic efficiency for 300 discharge-charge cycles at a current density of  $0.1 \text{ A g}^{-1}$  were investigated, which is more effective for the evaluation of the electrochemical performance of BSC. As depicted in Figure 8b, the reversible capacity was still kept at  $436.1 \text{ mA h g}^{-1}$  after 300 cycles, which is superior to NBSC, and the corresponding Coulombic efficiency was more than 92.0% after the first cycle, suggesting BSC as anode for LIB had excellent cyclic stability and reversibility. For BSC, the porous structure and the defects play an important role in the electrochemical performance. The relatively higher nitrogen content and specific surface area of BSC increase its conductivity and provide more contact sites and spaces between the electrolyte and BSC. In addition, we compared the electrochemical behavior of this study with other

reports (Table 2), and found that the electrochemical performance of the BSC anode is not always superior to them [16,25,46–48]. In this work, BSC showed superior electrochemical behavior with the two samples. The synergy of these factors made BSC as an anode achieve superior electrochemical performance than other biomass-based carbons [21,25,47,49,50].

**Table 2.** Comparison of carbon materials derived from biomass and their electrochemical performances as LIB anodes.

Carbon Source	Current Density (mA g <sup>-1</sup> )	Cycle Number	Reversible Capacity (mA h g <sup>-1</sup> )	Reference
Reed flowers	100	100	581.2	[16]
Coir pith waste	100	50	837	[46]
Walnut shell	100	200	280	[47]
Rice husks	100	100	429	[48]
Orange peel	1000	100	301	[25]
Bamboo shoot	100	100	449.9	This work
Bamboo shoot	100	300	436.1	This work

#### 4. Conclusions

Hierarchical porous nitrogen-doped carbon materials derived from bamboo shoot were obtained via a one-step or one-pot synthesis method in this work. This study demonstrates the substances in bamboo shoot, including proteins, carbohydrates, and minerals, make it a superior precursor for nitrogen-doped carbon materials for the storage of energy. The obtained carbon of BSC possessed a large specific surface area, different pore sizes from micro- to macropores, and retention of N at high temperatures. When used as the active material for LIB anodes, BSC exhibited superior specific capacities and rate capabilities than NBSC. These performances are related to the synergistic effect of the structures and functional groups of the obtained nitrogen-doped carbon material, which could enlarge the fields of the as-prepared nitrogen-doped carbons and form a promising material for energy storage.

**Author Contributions:** Z.L. designed the experiment. B.M. and H.L. prepared the samples, took characterization, B.M. and J.Y. took data analysis, discussed with W.H., C.J., X.L. and Y.L., B.M. wrote the manuscript, Y.L. and Z.L. revised the manuscript. All authors reviewed the manuscript. All authors have read and agreed to the published version of the manuscript.

**Funding:** This research was financially supported by the Basic Research Program of Natural Science of Shaanxi Province, China (Grant No. 2023-JC-QN-0247) and the Ph.D. Start-up Fund of Northwest A & F University, China (Grant No. 2452021068).

**Institutional Review Board Statement:** Not applicable.

**Informed Consent Statement:** Not applicable.

**Data Availability Statement:** Data are contained within the article.

**Conflicts of Interest:** The authors declare no conflict of interest.

#### References

1. Yan, L.T.; Rui, X.H.; Chen, G.; Xu, W.C.; Zou, G.F.; Luo, H.M. Recent advances in nanostructured Nb-based oxides for electrochemical energy storage. *Nanoscale* **2016**, *8*, 8443–8465. [[CrossRef](#)] [[PubMed](#)]
2. Reddy, M.V.; Rao, G.V.S.; Chowdari, B.V.R. Metal oxides and oxysalts as anode materials for Li ion batteries. *Chem. Rev.* **2013**, *113*, 5364–5457. [[CrossRef](#)] [[PubMed](#)]
3. Rehmana, J.; Fana, X.F.; Zheng, W.T. Computational insight of monolayer SnS<sub>2</sub> as anode material for potassium ion batteries. *Appl. Surf. Sci.* **2019**, *496*, 143625–143631. [[CrossRef](#)]
4. Peng, Q.; Rehman, J.; Eid, K.; Alofi, A.S.; Laref, A.; Albaqami, M.D.; Alotabi, R.G.; Shibl, M.F. Vanadium Carbide (V<sub>4</sub>C<sub>3</sub>) MXene as an efficient anode for Li-ion and Na-ion batteries. *Nanomaterials* **2022**, *12*, 2825–2836. [[CrossRef](#)]
5. Dahn, J.R.; Zheng, T.; Liu, Y.H.; Xue, J.S. Mechanisms for lithium insertion in carbonaceous materials. *Science* **1995**, *270*, 590–593. [[CrossRef](#)]

6. Liu, X.X.; Chao, D.L.; Li, Y.; Hao, J.; Liu, X.S.; Zhao, J.P.; Lin, J.Y.; Fan, H.J.; Shen, Z.X. A low-cost and one-step synthesis of N-doped monolithic quasi-graphene films with porous carbon frameworks for Li-ion batteries. *Nano Energy* **2015**, *17*, 43–51. [[CrossRef](#)]
7. Ren, M.M.; Yang, M.Z.; Liu, W.L.; Li, M.; Su, L.W.; Wu, X.B.; Wang, Y.H. Co-modification of nitrogen-doped graphene and carbon on  $\text{Li}_3\text{V}_2(\text{PO}_4)_3$  particles with excellent long-term and high-rate performance for lithium storage. *J. Power Sources* **2016**, *326*, 313–321. [[CrossRef](#)]
8. Ou, J.K.; Yang, L.; Zhang, Z.; Xi, X.H. Honeysuckle-derived hierarchical porous nitrogen, sulfur, dual-doped carbon for ultra-high rate lithium ion battery anodes. *J. Power Sources* **2016**, *333*, 193–202. [[CrossRef](#)]
9. Yu, W.H.; Wang, H.L.; Liu, S.; Mao, N.; Liu, X.; Shi, J.; Liu, W.; Chen, S.G.; Wang, X. N, O-codoped hierarchical porous carbons derived from algae for high-capacity supercapacitors and battery anodes. *J. Mater. Chem. A* **2016**, *4*, 5973–5983. [[CrossRef](#)]
10. Gopalakrishnan, A.; Kishore, K.R.; Sharma, C.S. A hybrid flexible N-doped candle-soot carbon nanofibers for binder-free lithium-ion battery anode. *Mater. Lett.* **2023**, *349*, 134873–134876. [[CrossRef](#)]
11. Selvamani, V.; Ravikumar, R.; Suryanarayanan, V.; Velayutham, D.; Gopukumar, S. Fish scale derived from nitrogen doped hierarchical porous carbon-a high rate performing anode for lithium ion cell. *Electrochim. Acta* **2015**, *182*, 1–10. [[CrossRef](#)]
12. Hou, J.H.; Cao, C.B.; Idrees, F.; Ma, X.L. Hierarchical porous nitrogen-doped carbon nanosheets derived from silk for ultrahigh-capacity battery anodes and supercapacitors. *ACS Nano* **2015**, *9*, 2556–2564. [[CrossRef](#)]
13. Zhou, X.; Wang, P.L.; Zhang, Y.G.; Wang, L.L.; Zhang, L.T.; Zhang, L.; Xu, L.; Liu, L. Biomass based nitrogen-doped structure-tunable versatile porous carbon materials. *J. Mater. Chem. A* **2017**, *5*, 12958–12968. [[CrossRef](#)]
14. Hu, C.G.; Xiao, Y.; Zhao, Y.; Chen, N.; Zhang, Z.P.; Cao, M.H.; Qu, L.T. Highly nitrogen-doped carbon capsules: Scalable preparation and high-performance applications in fuel cells and lithium ion batteries. *Nanoscale* **2013**, *5*, 2726–2733. [[CrossRef](#)] [[PubMed](#)]
15. Kan-nari, N.; Okamura, S.; Fujita, S.; Ozaki, J.; Arai, M. Nitrogen-doped carbon materials prepared by ammoxidation as solid base catalysts for Knoevenagel condensation and transesterification reactions. *Adv. Synth. Catal.* **2010**, *352*, 1476–1484. [[CrossRef](#)]
16. Zhao, W.M.; Wen, J.J.; Zhao, Y.M.; Wang, Z.F.; Shi, Y.R.; Zhao, Y. Hierarchically porous carbon derived from biomass reed flowers as highly stable Li-ion battery anode. *Nanomaterials* **2020**, *10*, 346–356. [[CrossRef](#)]
17. Li, X.N.; Liang, J.W.; Hou, Z.G.; Zhu, Y.C.; Qian, Y.T. Recycling chicken eggshell membranes for high-capacity sodium battery anodes. *RSC Adv.* **2014**, *4*, 50950–50954. [[CrossRef](#)]
18. Zhang, Y.Z.; Chen, L.; Meng, Y.; Xie, J.; Guo, Y.; Xiao, D. Lithium and sodium storage in highly ordered mesoporous nitrogen-doped carbons derived from honey. *J. Power Sources* **2016**, *335*, 20–30. [[CrossRef](#)]
19. Ou, J.K.; Zhang, Y.Z.; Chen, L.; Zhao, Q.; Meng, Y.; Guo, Y.; Xiao, D. Nitrogen-rich porous carbon derived from biomass as a high performance anode material for lithium ion batteries. *J. Mater. Chem. A* **2015**, *3*, 6534–6541. [[CrossRef](#)]
20. Selvamani, V.; Ravikumar, R.; Suryanarayanan, V.; Velayutham, D.; Gopukumar, S. Garlic peel derived high capacity hierarchical N-doped porous carbon anode for sodium/lithium ion cell. *Electrochim. Acta* **2016**, *190*, 337–345. [[CrossRef](#)]
21. Elizabeth, I.; Singh, B.P.; Trikha, S.; Gopukumar, S. Bio-derived hierarchically macro-meso-micro porous carbon anode for lithium/sodium ion batteries. *J. Power Sources* **2016**, *329*, 412–421. [[CrossRef](#)]
22. Lv, W.M.; Zhao, J.; Wen, F.S.; Xiang, J.Y.; Li, L.; Wang, L.M.; Liu, Z.Y.; Tian, Y.J. Carbonaceous photonic crystals as ultralong cycling anodes for lithium and sodium batteries. *J. Mater. Chem. A* **2015**, *3*, 13786–13793. [[CrossRef](#)]
23. Mondal, A.K.; Kretschmer, K.; Zhao, Y.F.; Liu, H.; Fan, H.B.; Wang, G.X. Naturally nitrogen doped porous carbon derived from waste shrimp shells for high-performance lithium ion batteries and supercapacitors. *Micropor. Mesopor. Mat.* **2017**, *246*, 72–80. [[CrossRef](#)]
24. Hu, X.D.; Sun, X.H.; Yoo, S.J.; Evanko, B.; Fan, F.R.; Cai, C.; Zheng, C.M.; Hu, W.B.; Stucky, G.D. Nitrogen-rich hierarchically porous carbon as a high-rate anode material with ultra-stable cyclability and high capacity for capacitive sodium-ion batteries. *Nano Energy* **2019**, *56*, 828–839. [[CrossRef](#)]
25. Mao, Y.; Duan, H.; Xu, B.; Zhang, L.; Hu, Y.S.; Zhao, C.C.; Wang, Z.X.; Chen, L.Q.; Yang, Y.S. Lithium storage in nitrogen-rich mesoporous carbon materials. *Energy Environ. Sci.* **2012**, *5*, 7950–7955. [[CrossRef](#)]
26. Xing, R.H.; Zhou, T.S.; Zhou, Y.; Ma, R.G.; Liu, Q.; Luo, J.; Wang, J.C. Creation of triple hierarchical micro-meso-macroporous N-doped carbon shells with hollow cores toward the electrocatalytic oxygen reduction reaction. *Nano-Micro Lett.* **2018**, *10*, 3. [[CrossRef](#)]
27. Xiang, J.Y.; Lv, W.M.; Mu, C.P.; Zhao, J.; Wang, B.C. Activated hard carbon from orange peel for lithium/sodium ion battery anode with long cycle life. *J. Alloys Compd.* **2017**, *701*, 870–874. [[CrossRef](#)]
28. Xu, G.Y.; Han, J.P.; Ding, B.; Nie, P.; Pan, J.; Dou, H.; Li, H.S.; Zhang, X.G. Biomass-derived porous carbon materials with sulfur and nitrogen dual-doping for energy storage. *Green Chem.* **2015**, *3*, 1668–1674. [[CrossRef](#)]
29. Chongtham, N.; Elangbam, D.; Manohar, L.S. Changes in nutrient components during ageing of emerging juvenile bamboo shoots. *Int. J. Food Sci. Nutr.* **2007**, *58*, 612–618.
30. Chongtham, N.; Bisht, M.S.; Haorongbam, S. Nutritional properties of bamboo shoots: Potential and prospects for utilization as a health food. *Compr. Rev. Food Sci. Food Saf.* **2011**, *10*, 153–168. [[CrossRef](#)]
31. Mi, B.B.; Chen, X.F.; Jiang, C.L.; Wang, J.X.; Chen, X.J.; Zhang, B.; Liu, X.M.; Liu, Z.J.; Fei, B.H. Nitrogen-doped porous carbon derived from bamboo shoot as solid base catalyst for Knoevenagel condensation and transesterification reactions. *Catalysts* **2018**, *8*, 232–241. [[CrossRef](#)]

32. Ding, J.; Wang, H.L.; Li, Z.; Cui, K.; Karpuzov, D.; Tan, X.H.; Kohandehghan, A.; Mitlin, D. Peanut shell hybrid sodium ion capacitor with extreme energy-power rivals lithium ion capacitors. *Energy Environ. Sci.* **2015**, *8*, 941–955. [[CrossRef](#)]
33. Pan, D.Y.; Wang, S.; Zhao, B.; Wu, M.H.; Zhang, H.J.; Wang, Y.; Jiao, Z. Li storage properties of disordered graphene nanosheets. *Chem. Mater.* **2009**, *21*, 3136–3142. [[CrossRef](#)]
34. Chen, L.; Zhang, Y.Z.; Lin, C.H.; Yang, W.; Meng, Y.; Guo, Y.; Li, M.L.; Xiao, D. Hierarchically porous nitrogen-rich carbon derived from wheat straw as an ultra-high-rate anode for lithium ion batteries. *J. Mater. Chem. A* **2014**, *2*, 9684–9690. [[CrossRef](#)]
35. Yan, Y.; Yin, Y.X.; Guo, Y.G.; Wan, L.J. A sandwich-like hierarchically porous carbon/graphene composite as a high-performance anode material for sodium-ion batteries. *Adv. Energy Mater.* **2014**, *4*, 1079–1098. [[CrossRef](#)]
36. Yang, Y.; Chen, D.M.; Han, W.B.; Cheng, Y.; Sun, B.Q.; Hou, C.L.; Zhao, G.D.; Liu, D.Z.; Chen, G.Q.; Han, J.C.; et al. Nature-inspired self-activation method for the controllable synthesis of highly porous carbons for high-performance supercapacitors. *Carbon* **2023**, *205*, 1–9. [[CrossRef](#)]
37. Wang, Q.H.; Lai, Z.Y.; Mu, J.; Chu, D.; Zang, X.R. Converting industrial waste cork to biochar as Cu (II) adsorbent via slow pyrolysis. *Waste Manag.* **2020**, *105*, 102–109. [[CrossRef](#)]
38. Li, Z.; Xu, Z.W.; Tan, X.H.; Wang, H.L.; Holt, C.M.; Stephenson, T.; Olsen, B.C.; Mitlin, D. Mesoporous nitrogen-rich carbons derived from protein for ultrahigh capacity battery anodes and supercapacitors. *Energy Environ. Sci.* **2013**, *6*, 871–878. [[CrossRef](#)]
39. Ma, C.C.; Shao, X.H.; Cao, D.P. Nitrogen-doped graphene nanosheets as anode materials for lithium ion batteries: A first-principles study. *J. Mater. Chem.* **2012**, *22*, 8911–8915. [[CrossRef](#)]
40. Liu, J.; Kopold, P.; van Aken, P.A.; Maier, J.; Yu, Y. Energy storage materials from nature through nanotechnology: A sustainable route from reed plants to a silicon anode for lithium-ion batteries. *Angew. Chem.* **2015**, *127*, 9768–9772. [[CrossRef](#)]
41. Pels, J.R.; Kapteijn, F.; Moulijn, J.A.; Zhu, Q.; Thomas, K.M. Evolution of nitrogen functionalities in carbonaceous materials during pyrolysis. *Carbon* **1995**, *33*, 1641–1653. [[CrossRef](#)]
42. Sevilla, M.; Parra, J.B.; Fuertes, A.B. Assessment of the role of micropore size and N-doping in CO<sub>2</sub> capture by porous carbons. *ACS Appl. Mater. Interfaces* **2013**, *5*, 6360–6368. [[CrossRef](#)] [[PubMed](#)]
43. Bhattacharjya, D.; Park, H.Y.; Kim, M.S.; Choi, H.S.; Inamdar, S.N.; Yu, J.S. Nitrogen-doped carbon nanoparticles by flame synthesis as anode material for rechargeable lithium-ion batteries. *Langmuir* **2014**, *30*, 318–324. [[CrossRef](#)]
44. Qie, L.; Chen, W.M.; Wang, Z.H.; Shao, Q.G.; Li, X.; Yuan, L.X.; Hu, X.L.; Zhang, W.X.; Huang, Y.H. Nitrogen-doped porous carbon nanofiber webs as anodes for lithium ion batteries with a superhigh capacity and rate capability. *Adv. Mater.* **2012**, *24*, 2047–2050. [[CrossRef](#)]
45. Zheng, F.C.; He, M.N.; Yang, Y.; Chen, Q.W. Nano electrochemical reactors of Fe<sub>2</sub>O<sub>3</sub> nanoparticles embedded in shells of nitrogen-doped hollow carbon spheres as high-performance anodes for lithium-ion batteries. *Nanoscale* **2015**, *7*, 3410–3417. [[CrossRef](#)]
46. Mullaivananathan, V.; Sathish, R.; Kalaiselvi, N. Coir pith derived bio-carbon: Demonstration of potential anode behavior in lithium-ion batteries. *Electrochim. Acta* **2017**, *225*, 143–150. [[CrossRef](#)]
47. Tao, L.; Huang, Y.B.; Zheng, Y.W.; Yang, X.Q.; Liu, C.; Di, M.W.; Larpiattaworn, S.; Nimlos, M.R.; Zheng, Z.F. Porous carbon nanofiber derived from a waste biomass as anode material in lithium-ion batteries. *J. Taiwan Inst. Chem. Eng.* **2019**, *95*, 217–226. [[CrossRef](#)]
48. Sekar, S.; Ahmed, A.A.; Inamdar, A.I.; Lee, Y.; Im, H.; Kim, D.Y.; Lee, S. Activated carbon-decorated spherical silicon nanocrystal composites synchronously-derived from rice husks for anodic source of lithium-ion battery. *Nanomaterials* **2019**, *9*, 1055–1067. [[CrossRef](#)]
49. Zhu, C.Y.; Akiyama, T. Cotton derived porous carbon via an MgO template method for high performance lithium ion battery anodes. *Green Chem.* **2016**, *18*, 2106–2114. [[CrossRef](#)]
50. Stephan, A.M.; Kumar, T.P.; Ramesh, R.; Thomas, S.; Jeong, A.K.; Nahm, K.S. Pyrolytic carbon from biomass precursors as anode materials for lithium batteries. *Mater. Sci. Eng. A* **2006**, *430*, 132–137. [[CrossRef](#)]

**Disclaimer/Publisher’s Note:** The statements, opinions and data contained in all publications are solely those of the individual author(s) and contributor(s) and not of MDPI and/or the editor(s). MDPI and/or the editor(s) disclaim responsibility for any injury to people or property resulting from any ideas, methods, instructions or products referred to in the content.